

THE *XMM-NEWTON* WIDE-FIELD SURVEY IN THE COSMOS FIELD. I. SURVEY DESCRIPTION

G. HASINGER,¹ N. CAPPELLUTI,¹ H. BRUNNER,¹ M. BRUSA,¹ A. COMASTRI,² M. ELVIS,³ A. FINOGENOV,¹ F. FIORE,⁴
A. FRANCESCHINI,⁵ R. GILLI,² R. E. GRIFFITHS,⁶ I. LEHMANN,¹ V. MAINIERI,^{1,7} G. MATT,⁸ I. MATUTE,^{1,9}
T. MIYAJI,⁶ S. MOLENDI,¹⁰ S. PALTANI,¹¹ D. B. SANDERS,¹² N. SCOVILLE,^{13,14} L. TRESSE,¹⁵
C. M. URRY,¹⁶ P. VETTOLANI,¹⁷ AND G. ZAMORANI²

Received 2006 April 24; accepted 2006 September 28

ABSTRACT

We present the first set of *XMM-Newton* EPIC observations in the 2 deg² COSMOS field. The strength of the COSMOS project is the unprecedented combination of a large solid angle and sensitivity over the whole multiwavelength spectrum. The *XMM-Newton* observations are very efficient in localizing and identifying active galactic nuclei (AGNs) and clusters, as well as groups of galaxies. One of the primary goals of the *XMM-Newton* Cosmos survey is to study the coevolution of active galactic nuclei as a function of their environment in the cosmic web. Here we present the log of observations, images, and a summary of first research highlights for the first pass of 25 *XMM-Newton* pointings across the field. In the existing data set we have detected 1416 new X-ray sources in the 0.5–2, 2–4.5, and 4.5–10 keV bands to an equivalent 0.5–2 keV flux limit of 7×10^{-16} erg cm⁻² s⁻¹. The number of sources is expected to grow to almost 2000 in the final coverage of the survey. From an X-ray color-color analysis we identify a population of heavily obscured, partially leaky or reflecting absorbers, most of which are likely to be nearby, Compton-thick AGNs.

Subject headings: cosmology: observations — large-scale structure of universe — dark matter — galaxies: formation — galaxies: evolution — X-rays: galaxies

1. INTRODUCTION

COSMOS is a global multiwavelength collaboration built around an *HST* Treasury Program providing deep images with the Advanced Camera for Surveys (ACS) that cover an unprecedentedly large contiguous 2 deg² field (Scoville et al. 2007). One of the primary goals of COSMOS is to study the coevolution of galaxies and their central black holes out to high redshifts, placing them in the context of the large-scale structure in which they reside and with high-resolution morphological information. The *XMM-Newton* observations are a crucial element of the

COSMOS survey because of the superb efficiency of X-ray observations in localizing and identifying active galactic nuclei (AGNs) and distant clusters of galaxies.

It has recently become clear that X-ray-selected AGNs are highly biased tracers of the dark matter distribution, as shown by the significant degree of angular autocorrelation and field-to-field variance in the source counts (Cappi et al. 2001; Cowie et al. 2002; Yang et al. 2003; Almaini et al. 2003; D’Elia et al. 2004; Cappelluti et al. 2005), as well as by the presence of spikes in the AGN redshift distribution, mapping onto the large-scale structure from optical data (Gilli et al. 2003; Barger et al. 2003). The evolution of the clustering with redshift and the comparison of the AGN clustering signal with that of other galaxy populations gives important information on the biasing of AGNs, and thus on the environment and type of dark matter halos in which activity is triggered. La Franca et al. (1998) reported the tentative detection of an increase of clustering of optically selected AGNs with redshift. The 2dF AGN survey found a factor of 2.7 increase of the clustering amplitude from $z = 0.5$ to 2.5 (Croom et al. 2005), based on a sample of more than 20,000 objects. The spatial clustering of X-ray-selected AGNs has recently been measured in different fields (Mullis et al. 2004a; Gilli et al. 2005; Yang et al. 2006), but the data so far are insufficient to obtain information on clustering evolution with redshift.

For a given survey area, the signal-to-noise ratio of the clustering signal scales with the surface density (for 2D correlation) or the volume density (for 3D correlation) of the objects in the sample. AGNs are very rare objects; however, deep X-ray surveys are known to yield the largest surface density of AGNs in any wave band (e.g., 1000 deg⁻² at the faintest limiting flux aimed for in the *XMM-Newton* COSMOS survey). Moreover, because X-rays both can penetrate obscuring dust and are not sensitive to dilution by starlight in the host galaxy, the X-ray selection of AGNs is not affected by some of the biases of the optical selection (see, e.g., Brandt & Hasinger 2005). The above-mentioned optical QSO correlation functions have been determined from surface densities of less than 30 AGNs deg⁻². The most recent deep optical surveys reach surface densities of

¹ Max Planck Institut für extraterrestrische Physik, P.O. Box 1312, D-85478 Garching, Germany.

² INAF-Osservatorio Astronomico di Bologna, via Ranzani 1, I-40127 Bologna, Italy.

³ Harvard-Smithsonian Center for Astrophysics, 60 Garden Street, Cambridge, MA 02138.

⁴ INAF-Osservatorio Astronomico di Roma, via Frascati 33, I-00044 Monteporzio Catone, Italy.

⁵ Dipartimento di Astronomia, Università di Padova, Vicolo dell’Osservatorio 2, I-35122 Padua, Italy.

⁶ Department of Physics, Carnegie Mellon University, 5000 Forbes Avenue, Pittsburgh, PA 15213.

⁷ European Southern Observatory, Karl-Schwarzschild-Strasse 2, D-85748 Garching bei München, Germany.

⁸ Dipartimento di Fisica, Università degli Studi Roma Tre, via della Vasca Navale 84, I-00146 Roma, Italy.

⁹ INAF-Osservatorio Astrofisico di Arcetri, Largo E. Fermi 5, I-50125 Firenze, Italy.

¹⁰ INAF/IASF-CNR, Sezione di Milano, via Bassini 15, I-20133 Milan, Italy.

¹¹ INTEGRAL Science Data Centre, Chemin d’Ecogia 16, CH-1290 Versoix, Switzerland.

¹² Institute for Astronomy, 2680 Woodlawn Drive, University of Hawaii, Honolulu, HI 96822.

¹³ California Institute of Technology, MC 105-24, 1200 East California Boulevard, Pasadena, CA 91125.

¹⁴ Visiting Astronomer, University of Hawaii, 2680 Woodlawn Drive, Honolulu, HI 96822.

¹⁵ Laboratoire d’Astrophysique de Marseille, BP 8, Traverse du Siphon, F-13376 Marseille Cedex 12, France.

¹⁶ Department of Astronomy, Yale University, P.O. Box 208101, New Haven, CT 06520-8101.

¹⁷ INAF-IRA, via Gobetti 101, I-40129 Bologna, Italy.

$\sim 250 \text{ deg}^{-2}$ in the case of COMBO-17 (Classifying Objects by Medium-Band Observations, a spectrophotometric 17-filter survey; Wolf et al. 2003), and $\sim 470 \text{ deg}^{-2}$ (Gavignaud et al. 2006) in the case of the Virgos-VLT Deep Survey (VVDS). The COMBO-17 survey contains 192 QSOs selected from intermediate-band photometric redshifts with $z_{\text{phot}} > 1.2$ and $17 < R_{\text{Vega}} < 24$ over 0.78 deg^2 , while the VVDS contains 74 spectroscopically selected QSOs in a solid angle of 0.6 deg^2 with $17.5 < I_{\text{AB}} < 24$. The large factor between the X-ray and the optical surface densities is crucial to map structures to a smaller scale than the ($1 h^{-1} \text{ Mpc}$) mapped with the current optical samples. Therefore, the most sensitive spatial clustering analysis of AGNs, especially at high redshift, will be obtained by an X-ray survey, which is both wide and deep simultaneously. In addition, an X-ray survey also including the hard (2–10 keV) band will give clustering information separately for the unabsorbed (type 1) and the absorbed (type 2) AGN populations and can thus directly test whether the obscured and unobscured AGNs originate from the same parent population of galaxies, a crucial ingredient in AGN unification scenarios. To study the 3D spatial correlation as a function of redshift and source class, a few hundred spectroscopically identified AGNs are required per class and redshift shell in a contiguous sky area. This is the main science goal of the *XMM-Newton* COSMOS Survey.

There is very good evidence that AGNs and galaxies co-evolve: the peaks of AGN activity and star formation occur in the same redshift range ($z = 1\text{--}2.5$), and there is a similar dramatic decline toward low redshift. Black hole mass and galactic bulge properties in the local universe are strongly correlated (Kormendy & Gebhardt 2001; Merrit & Ferrarese 2001). Therefore, the evolution of high-redshift AGNs can be utilized to study the formation and evolution of galaxies. The observed redshift distribution of faint X-ray sources (Cowie et al. 2003; Hasinger et al. 2003; Fiore et al. 2003; Ueda et al. 2003), both in the soft and the hard bands, peaks at $z \sim 0.7$ and is dominated by relatively low-luminosity objects ($\log L_X = 42\text{--}44 \text{ erg s}^{-1}$). Recently, the evolution of the space density of X-ray-selected AGNs has been derived (Hasinger et al. 2005) based on a sample of ~ 1000 type 1 AGNs selected in the 0.5–2 keV band from *ROSAT*, *XMM-Newton*, and *Chandra* deep surveys, with a very high completeness of optical redshift identification ($>97\%$). A strong dependence of the AGN space density evolution on X-ray luminosity has been found. The comoving space density of high-luminosity ($\log L_X > 44 \text{ erg s}^{-1}$) AGNs rises rapidly by more than a factor of 100 from $z = 0$ to $z \sim 2$, while the space density of low-luminosity AGNs evolves significantly less rapidly in the same redshift interval. Moreover, there is a clear increase of the peak redshift with increasing X-ray luminosity, both in the 0.5–2 keV and the 2–10 keV bands (Hasinger et al. 2003, 2005; Fiore et al. 2003; Ueda et al. 2003). Also, for the first time, there is firm evidence of a decline in the space density of lower luminosity AGNs toward higher redshift. This behavior was not recognized in previous, shallower surveys, e.g., from *ROSAT* (Miyaji et al. 2000), and was not included in the XRB synthesis models based on these (e.g., Gilli et al. 2001).

These new results paint a dramatically different evolutionary picture for low-luminosity AGNs compared to the high-luminosity QSOs. While the rare, high-luminosity objects can form and feed very efficiently rather early in the universe, with their space density declining more than 2 orders of magnitude at redshifts below $z = 2$, the bulk of the AGNs have to wait much longer to grow or to be activated, with a decline of space density by less than a factor of 10 below a redshift of 1. The late evolution of the low-luminosity Seyfert population is very similar to that required to fit the mid-infrared source counts and background (Franceschini

et al. 2002) and also the bulk of the star formation in the universe (Madau et al. 1998), while the rapid evolution of powerful QSOs more closely traces the history of formation of massive spheroids (Franceschini et al. 1999). This kind of antihierarchical black hole growth scenario is not predicted by most semianalytic galaxy evolution models based on cold dark matter structure formation (e.g., Kauffmann & Haehnelt 2000; Wyithe & Loeb 2003; Croton et al. 2005). It could indicate two modes of accretion and black hole growth with radically different accretion efficiency (see, e.g., the models of di Matteo et al. 2003; Merloni 2004; Menci et al. 2004).

The strong peak at $z = 0.7$ has been somewhat contested by Treister et al. (2004), who noted that the decline at high redshift is affected by a bias against the identification of distant obscured AGNs, while the obscured-to-unobscured AGN ratio at high z was still consistent with the value of $\sim 4:1$ observed locally. Indeed, $\sim 40\%$ of the local Seyfert galaxies are Compton thick (Risaliti et al. 1999). They are missing from all current X-ray surveys, but should show up in mid-infrared surveys due to their dust emission. On the other hand, the number of highly obscured objects missing in the current deep X-ray samples is limited by the integrated constraints on the number counts, the hard X-ray and soft gamma-ray background (Ueda et al. 2003), and the mass function of supermassive black holes in local galaxies (Marconi et al. 2004). Including the observed decrease of obscuration with increasing X-ray luminosity (Ueda et al. 2003; Hasinger 2004), there is an excellent consistency with all observed constraints (Ueda et al. 2003; Treister & Urry 2005; Gilli et al. 2007).

While the evolution of AGNs of all luminosity classes at $z < 2$ has now been firmly established from the rich X-ray samples discussed above, little is known about the growth phase of high-mass black holes in the redshift range 3–6. Unlike in the optical and radio bands, where a clear decline of the space density is observed in the redshift range 3–6 for the most luminous QSOs (Fan et al. 2001; Wall et al. 2005), no decrease in the space density of luminous X-ray QSOs is apparent up to $z = 4$ (Hasinger et al. 2005). Above that redshift, some evidence of a decline has been seen by Silverman et al. (2005) and Hasinger et al. (2005), but the number of objects available so far is much too small in comparison to the optical QSO surveys to obtain accurate quantitative information about the AGN growth phase. The total sample of AGNs more luminous than $\log L_X = 44$ at $z > 3$ that has been collected from all *ROSAT*, *Chandra*, and *XMM-Newton* surveys is just ~ 30 (Silverman et al. 2005; Steffen et al. 2004; Hasinger et al. 2005), while in the COSMOS survey, once completed, we expect of order 100 such objects, based on an extrapolation of the most recent type 1 AGN X-ray luminosity function (Hasinger et al. 2005). If large enough samples of AGNs (several hundred per unit redshift) can be spectroscopically identified, and their optical/NIR morphology can be studied with high angular resolution, then the well-known correlations between observable quantities of the host galaxies and nuclei, such as surface brightness profile, effective radius, and the stellar component velocity dispersion, which in the local universe is tightly correlated with the black hole mass (Kormendy & Gebhardt 2001; Merrit & Ferrarese 2001), open the possibility to extend these studies to high redshift and to truly determine the history of accretion in conjunction with galaxy formation.

Clusters and groups of galaxies represent the second most abundant class of objects identified in deep X-ray surveys. Due to their extended X-ray emission they can be easily discriminated from point sources. At redshifts $z < 1$ their rather low X-ray luminosities and temperatures correspond to groups and low-mass clusters. A handful of clusters with redshifts $z > 1$ has been

TABLE 1
XMM-Newton OBSERVING LOG FOR THE COSMOS FIELD

Target ^a	Observation Date	R.A. (J2000.0)	Decl. (J2000.0)	Exposure (ks)	GTI ^b (ks)	BKG Rate ^c (counts per 100 s)
Field 1	2004 Dec 11, 13:45:22	10 02 25	02 44 15	31.0	25.8	49.7
Field 2	2004 Dec 11, 22:58:42	10 02 25	02 29 16	44.0	12.3	48.7
Field 3	2005 May 14, 03:40:20	10 02 28	02 10 55	32.1	26.9	45.4
Field 4*	2004 Nov 21, 05:34:24	10 02 25	01 59 15	31.0	23.2	46.4
Field 5*	2004 Nov 21, 14:47:44	10 02 25	01 44 15	31.0	23.4	42.3
Field 6*	2004 May 30, 01:11:41	10 01 25	02 40 56	32.2	19.7	36.1
Field 7*	2003 Dec 6, 01:58:02	10 01 25	02 29 16	34.5	28.9	34.9
Field 8*	2004 Nov 17, 22:11:57	10 01 25	02 14 16	53.0	24.5	58.4
Field 9	2004 Nov 20, 01:08:49	10 01 25	01 59 15	36.2	18.6	44.4
Field 10*	2004 Nov 22, 00:01:05	10 01 25	01 44 15	45.5	11.5	45.0
Field 11	2004 Dec 1, 23:46:01	10 00 25	02 44 15	44.1	17.5	51.7
Field 12*	2003 Dec 8, 18:41:48	10 00 25	02 29 16	34.9	22.7	33.3
Field 13*	2003 Dec 10, 11:46:18	10 00 25	02 14 16	31.8	22.9	34.6
Field 14*	2003 Dec 10, 02:14:39	10 00 25	01 59 15	32.0	27.3	33.8
Field 15*	2004 Nov 19, 15:55:29	10 00 25	01 44 15	30.1	18.3	48.2
Field 16	2004 Dec 6, 01:17:33	09 59 25	02 42 36	40.1	0.0	126.8
Field 17	2004 Dec 11, 04:15:21	09 59 25	02 29 16	31.2	26.8	40.2
Field 18*	2003 Dec 12, 06:26:01	09 59 25	02 14 16	28.9	23.8	35.9
Field 19	2004 Dec 13, 21:59:19	09 59 25	01 59 15	30.1	20.9	36.7
Field 20	2005 May 14, 13:14:31	09 59 25	01 40 56	32.0	6.2	15.6
Field 21	2004 Dec 9, 07:38:16	09 58 25	02 44 15	62.6	54.0	39.4
Field 22*	2004 Nov 3, 06:24:56	09 58 25	02 29 16	31.0	25.3	65.5
Field 23	2005 May 9, 19:23:50	09 58 25	02 10 57	31.0	8.1	66.3
Field 24	2005 May 10, 04:37:10	09 58 25	01 55 58	31.0	15.5	60.8
Field 25	2005 May 10, 14:20:30	09 58 25	01 40 56	32.0	0.0	350.5

NOTE.—Units of right ascension are hours, minutes, and seconds, and units of declination are degrees, arcminutes, and arcseconds.

^a Entries marked with an asterisk are part of the 12 field sample, for which optical identifications are presented in Brusa et al. (2006).

^b Net exposure time in PN CCD good time intervals.

^c Average value of quiescent particle background in the 0.3–10 keV energy band after the cleaning.

discovered serendipitously in deep *ROSAT* (e.g., Rosati et al. 2002) and recently also in *XMM-Newton* observations. The highest redshift is at $z \sim 1.4$ (Mullis et al. 2005). At high luminosities the X-ray cluster population shows mild cosmological evolution, consistent with the growth of structure expected in a standard Λ CDM cosmology (Mullis et al. 2004b). At fainter X-ray fluxes considerable confusion can exist between the diffuse cluster emission and faint AGNs, either in the background or even as cluster members (e.g., Martini et al. 2006). Because of the strong cosmological AGN evolution, the likelihood of AGN contamination substantially increases with redshift. High angular resolution observations of some of the high-redshift clusters and a careful data analysis are thus important to understand possible biases introduced by AGN contamination.

Another population of objects discovered in deep X-ray fields are stars showing coronal emission, in particular G-, K-, and M-type stars with magnetic flaring activity. While at bright fluxes (e.g., in the *ROSAT* All-Sky Survey) coronal stars are quite abundant, the fraction of stars in the deep, high Galactic latitude fields is only a few percent, mainly because the observations are sensitive enough to reach beyond the typical stellar disk populations. Nevertheless, the statistics of stars in high-latitude fields can, e.g., constrain the decay of stellar magnetic activity on timescales of several Gyr (Feigelson et al. 2004).

In this paper (Paper I) we give an overview of the *XMM-Newton* survey in the COSMOS field, which is the basis for several accompanying publications in this *Supplement*, dealing with the X-ray data and the log N -log S (Paper II, Cappelluti et al. 2007), the optical identification and multiwavelength properties of a large sample of X-ray-selected sources (Paper III, Brusa

et al. 2006), the X-ray spectral properties of active galactic nuclei (Paper IV, Mainieri et al. 2007), the angular clustering of the X-ray point sources (Paper V, Miyaji et al. 2007), and statistical properties of clusters of galaxies (Paper VI, Finoguenov et al. 2007). Significant contributions from the XMM-Cosmos survey are also contained in the papers on a wide-angle tail galaxy in the COSMOS field, evidence for cluster formation (Smolcic et al. 2007) and on a large-scale structure at $z = 0.73$ and the relation of galaxy morphologies to the local environment (Guzzo et al. 2007).

2. *XMM-NEWTON* OBSERVATIONS

We have surveyed an area of 1.4×1.4 deg² within the region of sky bounded by $9^{\text{h}}57^{\text{m}}30^{\text{s}} < \text{R.A. (J2000.0)} < 10^{\text{h}}03^{\text{m}}30^{\text{s}}$; $1^{\circ}27'30'' < \text{decl. (J2000.0)} < 2^{\circ}57'30''$, which has also been covered almost completely by the *HSTACS* (1.67 deg²; see Leauthaud et al. 2007; Scoville et al. 2007). The observations with *XMM-Newton* (Jansen et al. 2001) cover a mosaic of 25 overlapping *XMM-Newton* pointings with a grid spacing of 15', i.e., about half of the size of the EPIC field of view. The EPIC cameras (Strüder et al. 2001; Turner et al. 2001) were operated in the standard full-frame mode. The thin filter was used for the PN camera and the medium filter for the MOS1 and MOS2 cameras. Table 1 gives a summary of the observations.

The PN and MOS data were preprocessed by the *XMM* Survey Scientist Consortium (Watson et al. 2001 SSC) using the *XMM-Newton* Standard Analysis System (SAS) routines. Because of software version changes, the data were reprocessed homogeneously at MPE using the SAS version 6.5.0 (see Cappelluti et al. 2007). A fraction of the observations were affected by high and

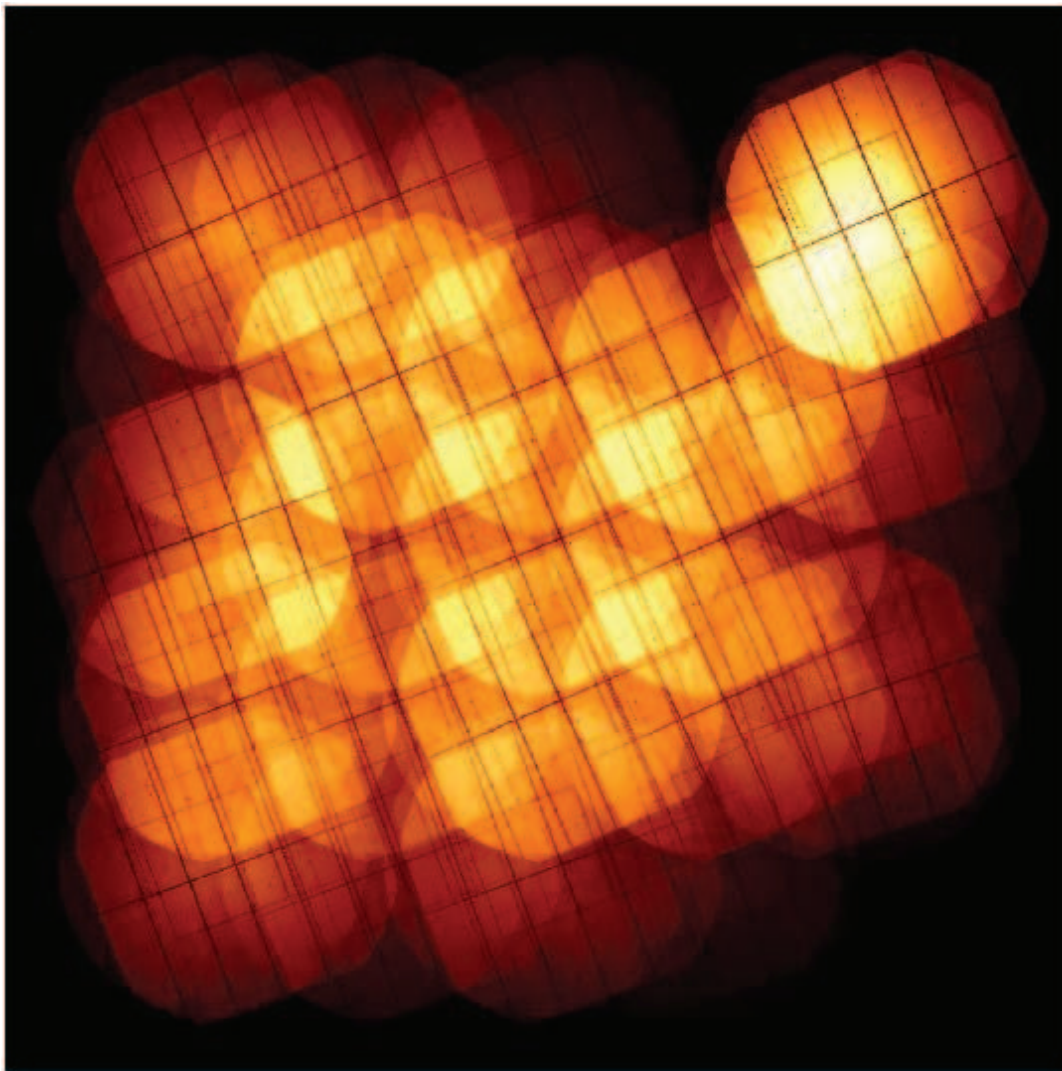


FIG. 1.—Exposure map of the *XMM-Newton* raster scan in the COSMOS field. The size of the field is about $1.4 \times 1.4 \text{ deg}^2$, centered at R.A. = $10^{\text{h}}00^{\text{m}}26.41^{\text{s}}$; decl. = $2^{\circ}12'36''$. North is up and east to the left. The 25 individual pointings specified in Table 1 run along successive columns from northeast to southwest.

flaring background fluxes with count rates up to several hundred per second, compared to a quiet count rate of several counts per second per detector. The data were screened for low background intervals, rejecting time intervals with more than 3σ enhancements in the background of the individual observation (Cappelluti et al. 2007). The remaining good time intervals for the PN CCD detector added up to about 504 ks (see Table 1). The requested exposure time for each pointing was 32 ks, but some fields were observed longer due to scheduling constraints. The actual exposure times for the three detectors, PN CCD, MOS1, and MOS2, are slightly different because of the different setup times. Two pointings (fields 16 and 25) were completely lost due to high background.

A number of hot pixels and hot columns were removed automatically from the event lists by the standard analysis software. We searched for additional hot pixels in images accumulated in detector coordinates, but did not find any. An exposure map for the whole mosaic of 23 pointings was calculated for the combination of PN CCD plus MOS1 and MOS2 cameras (Fig. 1). The map shows residual structure due to the inter-CCD gaps and dead pixels; however, the raster strategy with a $15'$ step significantly reduces the residual structures. We have been granted another pass over the COSMOS field with a total exposure time of 600 ks

in the next *XMM-Newton* observing period (AO4), thus almost doubling the existing data set. The remaining large-scale inhomogeneities due to missing pointings and variable net exposure times will be further smoothed out through the detailed planning of the upcoming observations. Because the pointing grid in AO4 will be shifted by $1'$ in both right ascension and declination, we also expect an additional smearing of the small-scale inhomogeneities. These AO4 observations have already started and have partly been used in the wavelet analysis for diffuse sources in Paper VI (Finoguenov et al. 2007). The full set of observations will be reported elsewhere after completion of the whole X-ray survey.

3. IMAGE ANALYSIS

An Al $K\alpha$ line at 1.5 keV is present in both detector types. The PN background spectrum shows in addition two strong copper lines at 7.4 and 8.0 keV, which are not present in the MOS background. PN photons in the energy ranges 7.2–7.6 and 7.8–8.2 keV, and all photons in the energy range 1.45–1.54 keV have therefore been neglected in the further analysis. For each separate pointing, images in celestial coordinates with a pixel size of $4''$ have been accumulated in the 0.5–2, 2–4.5, and 4.5–10 keV bands for all three detectors. These are the energy bands in which

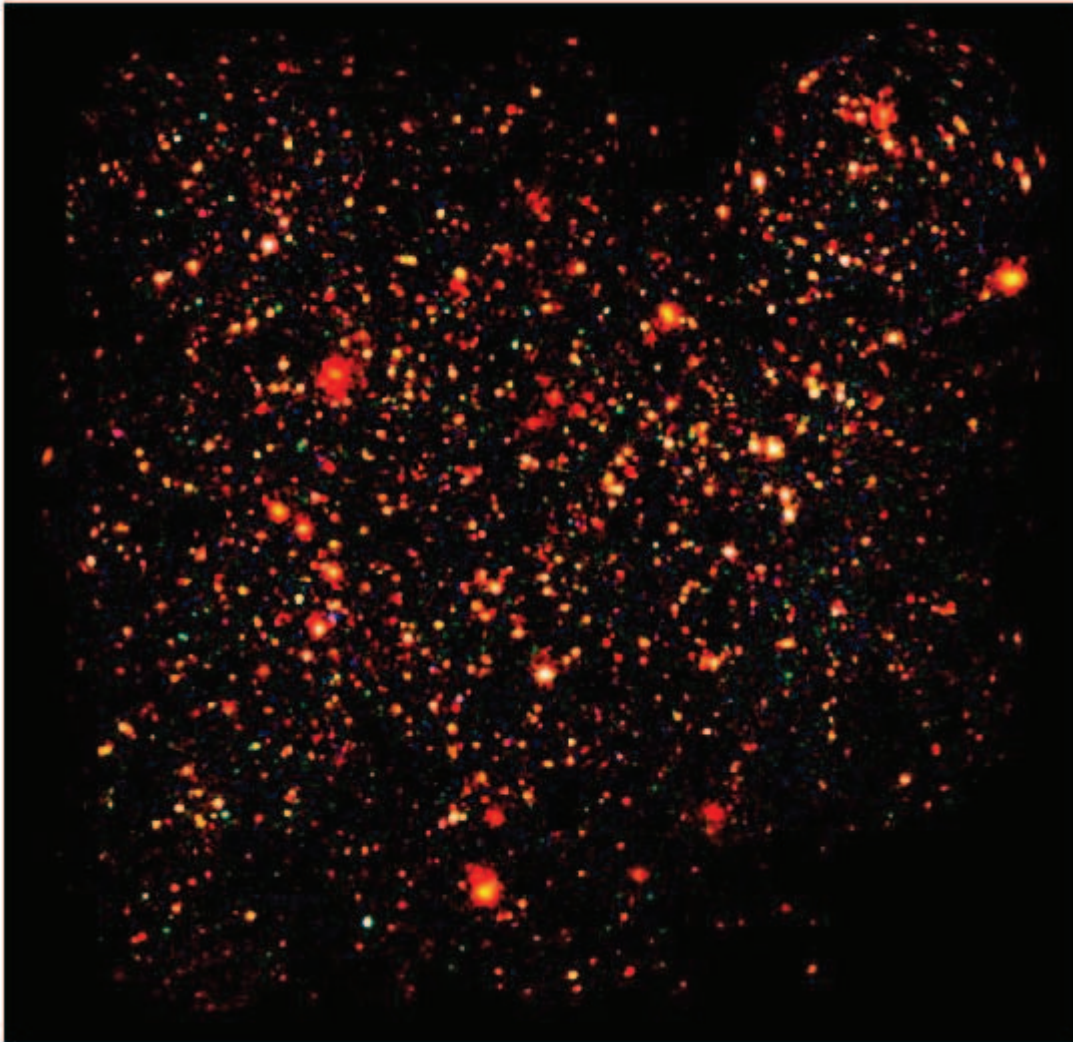


FIG. 2.—False-color X-ray image of the *XMM-Newton* raster survey in the COSMOS field. For each of the 23 individual pointings with good time intervals, raw images with $4''$ pixels have been accumulated in three different energy bands: 0.5–2 keV (*red*), 2–4.5 keV (*green*), and 4.5–10 keV (*blue*). These images were individually background-corrected and combined to a mosaic for all 23 pointings. Then they were filtered with a Gaussian kernel with a FWHM of $4''$.

the *XMM-Newton* Standard Analysis is performed and which have also been used in the first *XMM-Newton* publication on the number counts in the Lockman Hole (Hasinger et al. 2001). These bands are also rather close to the classical 0.5–2, 2–10, and 5–10 keV bands used in the literature, so that, given the energy-dependent sensitivity of imaging X-ray observatories, the counts-to-flux conversion has rather small systematic errors (see Hasinger et al. 2001). The images have been individually background-subtracted and then mosaicked to the full raster pointing (see Cappelluti et al. 2007 for more details).

Variations in the astrometric reference between different pointings are less than $2''$ and have been corrected for the current analysis. For each pointing the brighter X-ray sources have been statistically correlated to pointlike optical objects (i.e., AGNs or stars) using a maximum likelihood algorithm (*eposcorr* in SAS) to check the astrometry of the individual pointing images. Small corrections of order $2''$ – $3''$ in right ascension and declination were applied to the sky coordinates calculated from the original World Coordinate System keywords before jointly analyzing all pointings (Cappelluti et al. 2007). Combined PN+MOS1+MOS2 images were accumulated in the bands 0.2–0.5 keV (very soft), 0.5–2 keV (soft), 2–4.5 keV (hard), and 4.5–10 keV (very hard), respectively. Figure 2 shows the background-subtracted

image of all cameras combined in an X-ray false-color representation. The red, green, and blue colors refer to the soft, hard, and very hard images, respectively.

4. SUMMARY OF RESULTS

The source count rates from the 23-field COSMOS mosaic in the 0.5–2, 2–4.5, and 4.5–10 keV band have been converted to 0.5–2, 2–10, and 5–10 keV fluxes, respectively, and corresponding source counts have been derived in Cappelluti et al. (2007) together with the sky coverage for our observations. In this paper there is also an extensive discussion of systematic effects on the source counts, like source confusion and the Eddington bias. The $\log N$ - $\log S$ relations are nicely consistent with previous results from *ROSAT*, *ASCA*, *BeppoSAX*, *Chandra*, and *XMM-Newton*. However, at intermediate fluxes they have unprecedented statistical accuracy due to the large number of objects involved. The total number of sources (pointlike plus extended) detected in the 0.5–2, 2–10, and 5–10 keV bands are 1307, 735, and 187, respectively, and the corresponding flux limits are 0.7, 3.3, and 10×10^{-15} erg cm $^{-2}$ s $^{-1}$. The detection threshold has been set at a likelihood value of $L = -\ln(P_s) = 6$, where P_s is the probability for a spurious source detection. This corresponds roughly to a Gaussian confidence threshold of 4.5σ . The number of

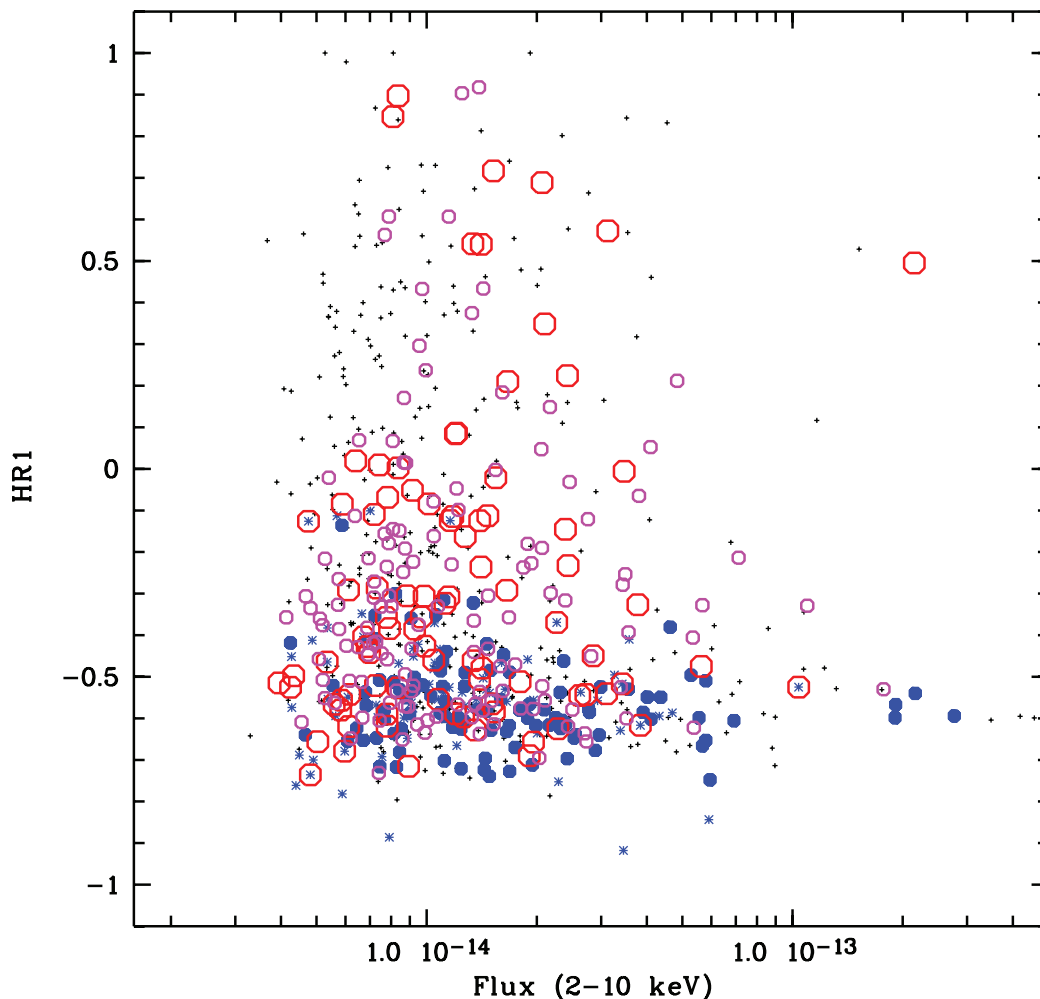


FIG. 3.—X-ray color-flux diagram of all sources detected in the 2–4.5 keV band in the COSMOS field. The 2–10 keV band flux (in $\text{erg cm}^{-2} \text{s}^{-1}$), calculated from the 2–4.5 keV band assuming a photon index $\Gamma = 1.7$, is plotted against the HR1 hardness ratio. Different symbols refer to the optical identification and classification of the sources. Filled circles are broad-line AGNs spectroscopically identified in the Magellan IMACS observations (Impey et al. 2007) and from the literature. Large open circles mark identified narrow emission line or absorption line galaxies. Asterisks and small open circles correspond to optical counterparts which are pointlike or resolved, respectively, in the *HST* ACS images of the first 12 optically identified fields (see Brusa et al. 2006). Dots are X-ray sources in the remaining 11 fields, for which optical identifications have not yet been attempted.

spurious sources in the total COSMOS survey depends on the number of statistically independent trials, which can only be calculated numerically for our detection scheme. Detailed Monte Carlo simulations of the *XMM-Newton* observations in the COSMOS field, using the realistic exposure time and background levels (Cappelluti et al. 2007), show that at this likelihood threshold about 33 spurious sources, i.e., about 2.4%, are expected among the whole X-ray catalog of the COSMOS field. This is consistent with similar simulations for the Lockman Hole (Brunner et al. 2006) and is also confirmed by the statistics of optically empty error circles in Brusa et al. (2006). The total number of different X-ray sources detected by the standard likelihood analysis method is 1416. The number of sources detected in the soft, hard, and very hard band only are 676, 89, and 3, respectively. The number of 1416 sources includes 26 objects that are found significantly extended by the maximum likelihood detection algorithm (Cappelluti et al. 2007).

First identifications with the optical catalogs from the Canada France Hawaii Telescope (CFHT) Megacam, Subaru SuprimCam, and *HST* ACS catalogs, as well as the UKIRT *K*-band catalog, are presented in accompanying Paper III (Brusa et al. 2006). Optical/

NIR candidates for the X-ray sources are identified using the *likelihood ratio technique*. This is a commonly used technique for associating objects in two catalogs with each other (Sutherland & Saunders 1992). It compares the probability that the object in question is the true counterpart, given the catalogued position errors, with the probability of finding a chance object with this magnitude at the position of this counterpart. The large majority of the X-ray sources can be readily identified with high likelihood using this procedure. Only rather small fractions of the X-ray sources cannot be uniquely identified, because the error circles either are empty down to the sensitivity of the optical/NIR images (6%), or contain multiple, about equally likely counterparts (4%). Spectroscopic identifications of the optical counterparts of the X-ray sources have started using the IMACS spectrograph at the Magellan telescope (Impey et al. 2007) and the VIMOS spectrograph at the VLT in the zCOSMOS survey (Lilly et al. 2007). Including about 40 spectroscopic identifications already in the literature, mainly from the 2dF and the SDSS surveys, a total of 377 X-ray sources could already be spectroscopically identified in the 23 *XMM-Newton* fields discussed here (see also Brusa et al. 2006).

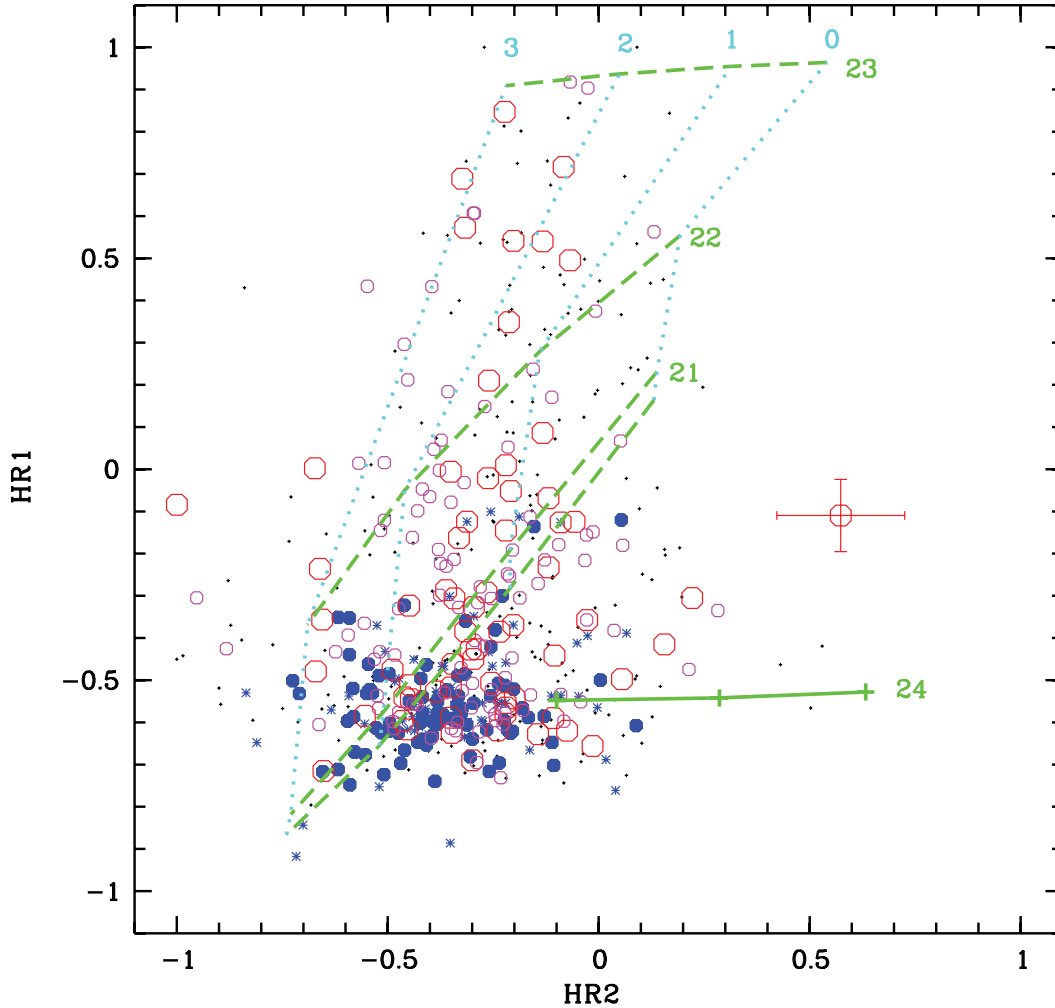


FIG. 4.— X-ray color-color diagram of the sources detected in the COSMOS field. For clarity, only those sources are plotted for which the errors in HR1 and HR2 are less than 0.25. One representative set of error bars has been plotted for the source with XID 2608, which is discussed specifically in the text. The symbols are the same as in Figure 3. The grid lines refer to spectral models simulated using XSPEC. Dashed and dotted lines show simple power-law spectra with photon indices $\Gamma = 0, 1, 2, 3$ and intrinsic absorption (in the observed frame) of $\log N_{\text{H}} = 21, 22, 23 \text{ cm}^{-2}$ indicated in the diagram. The grid line for $\log N_{\text{H}} = 0 \text{ cm}^{-2}$ is slightly below that for $\log N_{\text{H}} = 21 \text{ cm}^{-2}$. The solid line corresponds to a reflection or leaky absorber model with photon index of 1.7 with intrinsic absorption of $N_{\text{H}} = 10^{24} \text{ cm}^{-2}$. The ticks along the line indicate the unabsorbed flux percentage of 1%, 3%, and 10% (from right to left).

Hardness ratios have been calculated from the counts in the three different energy bands in the classical way:

$$\text{HR} = (H - S)/(H + S).$$

Below, HR1 refers to the hard versus soft band and HR2 to the very hard versus the hard band. Figure 3 shows an X-ray color-intensity diagram based on the 2–10 keV fluxes. Different symbols indicate different types of sources. It is easy to see that spectroscopically identified broad-line AGNs (*filled circles*), as well as X-ray sources with pointlike ACS counterparts (*asterisks*) only populate the soft part of the diagram, with hardness ratios typically in the range $\text{HR1} < -0.2$. These are candidate type 1 AGNs. Sources spectroscopically identified with narrow emission or absorption lines (*large open circles*), as well as resolved ACS counterparts (*small open circles*) populate the whole hardness ratio range. These are either candidate type 2 AGNs (mainly those with hard X-ray spectra) or low-luminosity type 1 AGNs whose optical light is dominated by the host galaxy.

Figure 4 shows an X-ray color-color diagram for the same sources. For clarity we plotted only sources with reasonably small

errors in the hardness ratio and that are significantly detected either in the hard or the very hard band (see caption). The grid of dashed and dotted lines, as well as the single solid line, show different power-law models folded through the instrument response of PN+MOS1+MOS2. As already found in Hasinger et al. (2001) and Della Ceca et al. (2004), type 1 AGNs cluster in a well-defined location in this diagram, corresponding to low intrinsic absorption and spectral photon indices close to 1.7–2. The fact that the median of the type 1 AGNs is shifted slightly to the right of the $N_{\text{H}} = 0$ line may indicate the presence of additional soft components in some of the spectra. Type 2 AGNs tend to have larger hardness ratios, especially in HR1, corresponding to larger intrinsic absorption values. Interestingly, there is a group of sources, putative type 2 AGNs with quite hard colors in the hard band (HR2), but hardness ratios consistent with unabsorbed sources in the soft band, which do not fit any of the simple power law plus absorption models. The solid model track shows, however, that their colors can be reconciled with heavily absorbed low-redshift sources with some fraction (1%–10%) of unabsorbed flux leaking out. At higher redshifts, the intrinsically absorbed continua move to a softer band, so that these objects

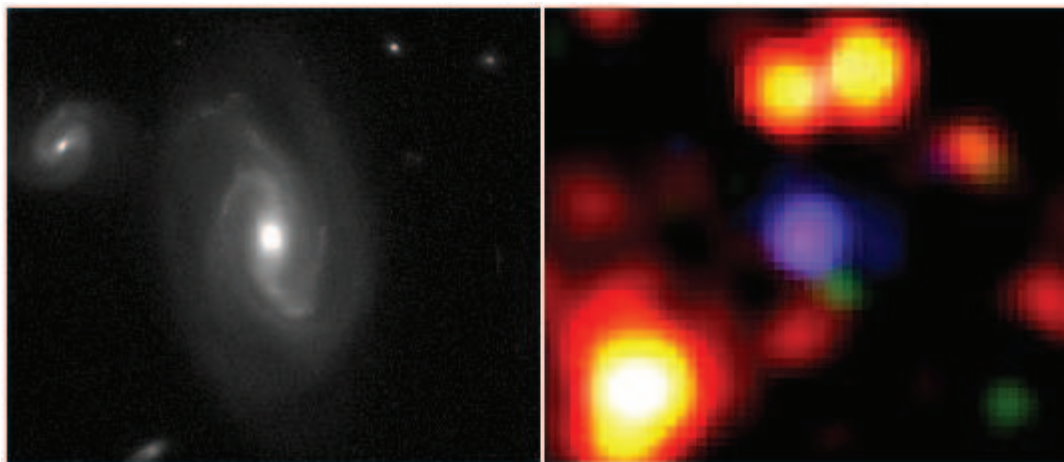


FIG. 5.—*Left:* *HST* ACS cutout centered on the spiral galaxy 2MASX J10014194+0203577 from the COSMOS ACS coverage (Scoville et al. 2007), corresponding to XID 2608, the hardest spectroscopically identified X-ray source in the current *XMM-Newton* coverage of COSMOS. This galaxy has an ACS *I*-band magnitude of 16.1 and a 2MASS *K*-band magnitude of 13.2. The redshift measured by the SDSS is 0.1248. There is a nearby counterpart, possibly weakly interacting. The image is $30''$ across. *Right:* Cutout of the X-ray false color image in Figure 2, centered on XID 2608. The image is approximately $3'$ across. The peculiar spectrum of the X-ray source is immediately apparent in the violet color, which indicates contributions from the soft and the very hard band, but little contribution from the hard band.

would shift to a different place in the color-color diagram (Guainazzi et al. 2005). A single prototypical object (source 901) has already been discovered in the *XMM-Newton* observations of the Lockman Hole (Mainieri et al. 2002). Guainazzi et al. (2005) have recently shown that bright, local, Compton-thick Seyfert 2 galaxies populate the same area in the color-color diagram. The large solid angle coverage of the COSMOS field now clearly identifies them as a population of the probably most absorbed objects in the field. Using the tentative criterion of $\text{HR2} > 0.1$ and $\text{HR1} < -0.1$, a total of 18 candidates can be selected, which is $\sim 3\%$ of the total number of objects shown in Figure 4, a fraction consistent with that detected in the Lockman Hole (Hasinger et al. 2001). Mainieri et al. (2007) elaborate on the spectral analysis of individual sources, concentrating on the brighter spectroscopically identified sources in the COSMOS field.

A particularly interesting source is XID 2608, the source with the largest HR2 ratio among those spectroscopically identified in Figure 4. It is a galaxy with a redshift $z = 0.125$ from the SDSS archive and an *I*-band magnitude of 16.11 (Brusa et al. 2006). Combining all three EPIC cameras, it has 72.4, 43.1, and 133.3 net counts in the soft, hard, and very hard band, respectively, and thus a very peculiar X-ray spectrum. The 5–10 keV flux derived from the counts in the very hard band is $\sim 4 \times 10^{-14}$ ergs cm^{-2} s^{-1} , corresponding to a 5–10 keV luminosity of 1.3×10^{43} erg s^{-1} . Figure 5 shows a cutout from the ACS mosaic on the left and a zoom into the X-ray false color image on the right. The peculiar X-ray spectrum of this possibly weakly interacting spiral galaxy is immediately apparent from its strange violet X-ray color. A high-quality optical spectrum for this source is available in the SDSS archive and has been analyzed by Kauffmann et al. (2003) as part of their massive spectral analysis of all SDSS emission line galaxies. It has been classified by these authors as a narrow-line Seyfert galaxy with moderate power [$\log(L_{[\text{O III}]}) = 6.45$]. The host galaxy is rather massive with a stellar mass around $(2-3) \times 10^{11} M_{\odot}$ and a stellar velocity dispersion of $\sigma_v \sim 160$ km s^{-1} . Despite its absence in the total spectrum, a significant $\text{H}\beta$ emission line is found by these authors in the residual AGN spectrum after subtraction of the appropriate galaxy spectrum. The diagnostic line ratios $\log[\text{O III}]/\text{H}\beta = 0.61$ and $\log[\text{N II}]/\text{H}\alpha = 0.12$ put this object among the bulk of the normal Seyfert 2 galaxies. With its X-ray and $[\text{O III}]$ luminosity

and its peculiar X-ray spectrum, the object can be identified as a heavily absorbed, moderately powerful Seyfert 2 galaxy, with a soft component from a leaky absorber, a scatterer/reflection nebula (Elvis et al. 1983), or a circumnuclear starburst region.

First science results from the *XMM-Newton* survey of the COSMOS field have also been derived in the realm of large-scale structure and clusters of galaxies. A survey of clusters and groups of galaxies, based on extended X-ray sources detected by a wavelet algorithm in the data set of 36 *XMM-Newton* pointings and overdensities in optical photometric redshift catalogs, has detected 72 candidate groups and clusters over the whole field (Scoville et al. 2007; Finoguenov et al. 2007), the most massive of which have independently been confirmed through a weak-lensing analysis (Massey et al. 2007). These results provide first constraints on the number counts and mass function of groups and clusters in this so-far unexplored flux range. A particularly interesting group of clusters has been found at a redshift around $z = 0.73$ (Guzzo et al. 2007). A first angular correlation function of the active galactic nuclei in the 23-field survey finds a significant signal in the range $\sim 0.5' - 20'$ in all three energy bands of 0.5–2, 2–4.5, and 4.5–10 keV (Miyaji et al. 2007).

5. PUBLIC DATA RELEASE

The COSMOS *XMM-Newton* data are publicly available in staged releases through the web sites at MPE¹⁸ and at IPAC/IRSA.¹⁹ The *XMM-Newton* pipeline processed data are of course also available in the *XMM-Newton* archive.

This work is based on observations obtained with *XMM-Newton*, an ESA science mission with instruments and contributions directly funded by ESA Member States and the US (NASA). In Germany, the *XMM-Newton* project is supported by the Bundesministerium für Bildung und Forschung/Deutsches Zentrum für Luft und Raumfahrt, and the Max-Planck Society. Part of this work was supported by the Deutsches Zentrum für

¹⁸ See <http://www.mpe.mpg.de/XMMCosmos/23fields/>.

¹⁹ See <http://irsa.ipac.caltech.edu/data/COSMOS/>.

Luft- und Raumfahrt, DLR project numbers 50 OR 0207 and 50 OR 0405. We gratefully acknowledge the contributions of the entire COSMOS collaboration consisting of more than 100 scientists. More information on the COSMOS survey is available at <http://www.astro.caltech.edu/cosmos>. This re-

search has made use of the NASA/IPAC Extragalactic Database (NED) and the SDSS spectral archive. We thank Guinevere Kauffmann and Jarle Brinchmann for help with the object No. 2608. We acknowledge helpful comments from an anonymous referee.

REFERENCES

- Almaini, O., et al. 2003, *MNRAS*, 338, 303
 Barger, A. J., et al. 2003, *AJ*, 126, 632
 Brandt, W. N., & Hasinger, G. 2005, *ARA&A*, 43, 827
 Brunner, H., et al. 2007, *ApJ*, submitted
 Brusa, M., et al. 2007, *ApJS*, 172, 353 (Paper III)
 Cappelluti, N., Cappi, M., Dadina, M., Malaguti, G., Branchesi, M., D'Elia, V., & Palumbo, G. G. C. 2005, *A&A*, 430, 39
 Cappelluti, N., et al. 2007, *ApJS*, 172, 341 (Paper II)
 Cappi, M., et al. 2001, *ApJ*, 548, 624
 Cowie, L. L., Barger, A. J., Bautz, M. W., Brandt, W. N., Garmire, G. P. 2003, *ApJ*, 584, L57
 Cowie, L. L., Garmire, G. P., Bautz, M. W., Barger, A. J., Brandt, W. N., Hornschemeier, A. E. 2002, *ApJ*, 566, L5
 Croom, S. M., et al. 2005, *MNRAS*, 356, 415
 Croton, D. J., et al. 2006, *MNRAS*, 365, 11
 D'Elia, V., Fiore, F., Elvis, M., Cappi, M., Mathur, S., Mazzotta, P., Falco, E., & Cocchia, F. 2004, *A&A*, 422, 11
 Della Ceca, R., et al. 2004, *A&A*, 428, 383
 di Matteo, T., Croft, R. A. C., Springel, V., & Hernquist, L. 2003, *ApJ*, 593, 56
 Elvis, M., Briel, U. G., & Henry, J. P. 1983, *ApJ*, 268, 105
 Fan, X., et al. 2001, *AJ*, 121, 54
 Feigelson, E. D., & Lawson, W. A. 2004, *ApJ*, 614, 267
 Finoguenov, A., et al. 2007, 172, 182 (Paper VI)
 Fiore, F., et al. 2003, *A&A*, 409, 79
 Franceschini, A., Braito, V., & Fadda, D. 2002, *MNRAS*, 335, L51
 Franceschini, A., Hasinger, G., Miyaji, T., & Malquori, D. 1999, *MNRAS*, 310, L5
 Gavignaud, I., et al. 2006, *A&A*, 457, 79
 Gilli, R., Comastri, A., & Hasinger, G. 2007, *A&A*, 463, 79
 Gilli, R., Salvati, M., & Hasinger, G. 2001, *A&A*, 366, 407
 Gilli, R., et al. 2003, *ApJ*, 592, 721
 ———. 2005, *A&A*, 430, 811
 Guainazzi, M., Matt, G., & Perola, G. C. 2005, *A&A*, 444, 119
 Guzzo, L., et al. 2007, *ApJS*, 172, 254
 Hasinger, G. 2003, in *AIP Conf. Proc. 666, The Emergence of Cosmic Structure: Thirteenth Astrophysics Conference*, ed. S. Holt, F. Olin, & C. Reynolds (New York: AIP), 227
 Hasinger, G. 2004, *Nucl. Phys. B Proc. Supp.*, 132, 86
 Hasinger, G., Miyaji, T., & Schmidt, M. 2005, *A&A*, 441, 417
 Hasinger, G., et al. 2001, *A&A*, 365, L45
 Impey, C., et al. 2007, *ApJS*, submitted
 Jansen, F., et al. 2001, *A&A*, 365, L1
 Kauffmann, G., & Haehnelt, M. G. 2000, *MNRAS*, 311, 576
 Kauffmann, G., et al. 2003, *MNRAS*, 346, 1055
 Kormendy, J., & Gebhardt, K. 2001, in *AIP Conf. Proc. 586, 20th Texas Symposium on Relativistic Astrophysics*, ed. J. C. Wheeler & H. Martel (Melville: AIP), 363
 La Franca, F., Andreani, P., & Cristiani, S. 1998, *ApJ*, 497, 529
 Leauthaud, A., et al. 2007, *ApJS*, 172, 219
 Lilly, S., et al. 2007, *ApJS*, 172, 70
 Madau, P., Pozzetti, L., & Dickinson, M. 1998, *ApJ*, 498, 106
 Mainieri, V., Bergeron, J., Hasinger, G., Lehmann, I., Rosati, P., Schmidt, M., Szokoly, G., & Della Ceca, R. 2002, *A&A*, 393, 425
 Mainieri, V., et al. 2007, *ApJS*, 172, 368 (Paper IV)
 Marconi, A., Risaliti, G., Gilli, R., Hunt, L. K., Maiolino, R., Salvati, M. 2004, *MNRAS*, 351, 169
 Martini, P., Kelson, D., Kim, E., Mulchaey, J., Athey, A. 2006, *ApJ*, 644, 116
 Massey, R., et al. 2007, *Nature*, 445, 286
 Menci, N., Fiore, F., Perola, G. C., & Cavaliere, A. 2004, *ApJ*, 606, 58
 Merloni, A. 2004, *MNRAS*, 353, 1035
 Merrit, D., & Ferrarese, L. 2001, *MNRAS*, 320, L30
 Miyaji, T., Hasinger, G., & Schmidt, M. 2000, *A&A*, 353, 25
 Miyaji, T., et al. 2007, *ApJS*, 172, 396 (Paper V)
 Mullis, C. R., Henry, J. P., Gioia, I. M., Böhringer, H., Briel, U. G., Voges, W., & Huchra, J. P. 2004a, *ApJ*, 617, 192
 Mullis, C. R., Rosati, P., Lamer, G., Böhringer, H., Schwobe, A., Schuecker, P., & Fassbender, R. 2005, *ApJ*, 623, L85
 Mullis, C. R., et al. 2004b, *ApJ*, 607, 175
 Risaliti, G., Maiolino, R., & Salvati, M. 1999, *ApJ*, 522, 157
 Rosati, P., Borgani, S., & Norman, C. 2002, *ARA&A*, 40, 539
 Scoville, N., et al. 2007, *ApJS*, 172, 1
 Silverman, J. D., et al. 2005, *ApJ*, 624, 630
 Smolcic, V., et al. 2007, *ApJS*, 172, 295
 Steffen, A. T., Barger, A. J., Capak, P., Cowie, L. L., Mushotzky, R. F., Yang, Y. 2004, *AJ*, 128, 1483
 Strüder, L., et al. 2001, *A&A*, 365, L18
 Sutherland, W., & Saunders, W. 1992, *MNRAS*, 259, 413
 Treister, E., & Urry, C. M. 2005, *ApJ*, 630, 115
 Treister, E., et al. 2004, *ApJ*, 616, 123
 Turner, M. J. L., et al. 2001, *A&A*, 365, L27
 Ueda, Y., Akiyama, M., Ohta, K., & Miyaji, T. 2003, *ApJ*, 598, 886
 Wall, J. V., Jackson, C. A., Shaver, P. A., Hook, I. M., & Kellermann, K. I. 2005, *A&A*, 434, 133
 Watson, M. G., et al. 2001, *A&A*, 365, L51
 Wolf, C., Wisotzki, L., Borch, A., Dye, S., Kleinheinrich, M., & Meisenheimer, K. 2003, *A&A*, 408, 499
 Wyithe, J. S. B., & Loeb, A. 2003, *ApJ*, 595, 614
 Yang, Y., Mushotzky, R. F., Barger, A. J., & Cowie, L. L. 2006, *ApJ*, 645, 68
 Yang, Y., Mushotzky, R. F., Barger, A. J., Cowie, L. L., Sanders, D. B., Steffen, A. T. 2003, *ApJ*, 585, L85